Clim. Past Discuss., 7, 1261–1299, 2011
www.clim-past-discuss.net/7/1261/2011/
doi:10.5194/cpd-7-1261-2011

Climate of the Past Discussions

Glacial marine carbon cycle sensitivities to Atlantic ocean circulation reorganization by coupled climate model simulations

M. O. Chikamoto[1], A. Abe-Ouchi[1,2], A. Oka[2], R. Ohgaito[1], and A. Timmermann[3]

[1]Research Institute for Global Change, Japan Agency for Marine-Earth Science and Technology, Yokohama, Kanagawa, Japan
[2]Atmosphere and Ocean Research Institute, University of Tokyo, Kashiwa, Chiba, Japan
[3]International Pacific Research Center, University of Hawaii, Honolulu, Hawaii, USA

Received: 1 April 2011 – Accepted: 4 April 2011 – Published: 13 April 2011

Correspondence to: M. O. Chikamoto (megchika@jamstec.go.jp)

Published by Copernicus Publications on behalf of the European Geosciences Union.

Abstract

A series of Last Glacial Maximum (LGM) marine carbon cycle sensitivity experiments is conducted to test the effect of different physical processes, as simulated by two atmosphere-ocean general circulation model (AOGCM) experiments, on the atmospheric pCO_2. One AOGCM solution exhibits an increase in North Atlantic Deep Water (NADW) formation, whereas the other mimics an increase in Antarctic Bottom Water (AABW) associated with a weaker NADW. Due to enhanced gas solubility associated with lower sea surface temperature, both experiments generate a reduction of atmospheric pCO_2 by about 20–23 ppm. However, neither a weakening of NADW nor an increase of AABW formation causes a large atmospheric pCO_2 change. A marked enhancement in AABW formation is required to represent the reconstructed vertical gradient of dissolved inorganic carbon (DIC) during LGM conditions. The efficiency of Southern Ocean nutrient utilization reduces in response to an enhanced AABW formation, which counteracts the circulation-induced ocean carbon uptake.

1 Introduction

During the late Pleistocene, the global temperatures and atmospheric carbon dioxide (CO_2) concentrations varied on 80–120 kyr glacial-interglacial timescale (e.g., Petit et al., 1999; Siegenthaler et al., 2005). Despite the prominent relationship between climate and the carbon cycle, the mechanisms controlling the glacial-interglacial pCO_2 variations are still unresolved (Sigman and Boyle, 2000; Archer et al., 2000). Compared to present-day condition, terrestrial carbon stocks were reduced considerably during glacial conditions, due to more arid climate conditions and the extensive land ice coverage (Crowley, 1995). Accordingly, the marine carbon cycle must have been the main driver for lowering atmospheric pCO_2 by 80–100 ppm during glacial periods.

There is likely to be, not one, but several candidates for explaining the reduction in glacial atmospheric CO_2 level (Archer et al., 2000; Sigman and Boyle, 2000; Köhler

CPD
7, 1261–1299, 2011

et al., 2005). One contributor to the glacial CO_2 decrease is an increase in the solubility of CO_2 gas (Bacastow and Maier-Reimer, 1990). It has been estimated that during glacial periods, a cooling of the surface oceans led to a global CO_2 drawdown of 25–30 ppm through enhanced solubility in sea water (Sigman and Boyle, 2000; Kohfeld and Ridgwell, 2009). Understanding what caused the remaining drop of 75 ppm is an important quest that has been based on a hierarchy of climate-carbon cycle modelling studies.

The reorganization of ocean circulation during the glacial periods has been suggested to affect the ocean carbon cycle and hence drives atmospheric pCO_2 changes. According to high salinity glacial pore waters (Adkins et al., 2002), deep and bottom water ventilation may have been reduced during the Last Glacial Maximum (LGM). A weakening of ventilation and/or vertical mixing around Antarctica would enhance Southern Ocean stratification, which may contribute to a reduction of atmospheric CO_2 by over 20 ppm (Peacock et al., 2006; Watson and Naveira Garabato, 2006; Gildor et al., 2002). These studies support the notion that lowering ventilation enhances deep-ocean stratification, leading to a large vertical gradient in the dissolved inorganic carbon (DIC). Furthermore, Bouttes et al. (2010, 2011) argue that an increase of denser Antarctic Bottom Water (AABW) formation reduces the carbon exchange between upper and deeper ocean and subsequently decreases atmospheric pCO_2. Potential shifts of deep-water formation from the North Atlantic to the Southern Ocean may lead to changes in the efficiency of oceanic carbon uptake by ocean biology (Ito and Follows, 2005). An increase in the Southern Ocean deep-water formation reorganizes the available utilized nutrients at the surface, weakening biological production and therefore oceanic carbon uptake (Marinov et al., 2008). These results suggest that an explicit representation of the deep-water formation in both polar regions may be an important element in the marine carbon cycle response to glacial-interglacial climate change.

The interaction between ocean circulation and sea-ice coverage in the atmosphere-ocean system may also play an important role for the LGM marine carbon cycle and atmospheric pCO_2. Sea-ice coverage, production and the related brine formation are

CPD
7, 1261–1299, 2011

strongly related to the deep-ocean ventilation and polar convection. In an LGM box model study, sea ice expansion near 55° S prevents carbon release in the Southern Ocean, thereby reducing pCO_2 to 215 ppm (Stephens and Keeling, 2000). Winter sea ice also expands in the subpolar North Atlantic (de Vernal et al., 2006) and may further modulate atmospheric pCO_2. Changes in sea-ice coverage also affect biological productivity. An idealized linear increase in sea-ice extent shows the buildup of atmospheric CO_2 due to weakened biological productivity by light limitation (Archer et al., 2003; Kurahashi-Nakamura et al., 2007).

The glacial-interglacial variability in atmospheric pCO_2 has been studied using idealized and/or glacial Sea Surface Temperature (SST) forcings in box-type and intermediate complexity earth system models (Brovkin et al., 2007). Due to their low complexity and computational costs, these studies have explored a range of carbon-cycle responses, at the expense, however, of well-resolved physics. Moreover, sets of glacial-interglacial simulations using AOGCMs have been carried outin Paleoclimate Model Intercomparison Project phase 2 (PMIP2). These experiments provide a deeper insight into interaction between ocean circulation and sea ice during the last glacial period.

In this study, we use a series of AOGCM simulations that represent glacial characteristics of ocean circulation and sea-ice coverage and then evaluate the climate dynamical effects on the marine carbon cycle using an offline ocean biogeochemical model. The method applied here enables us to evaluate multiple simulations of the past, present, and future ocean carbon cycle according to AOGCM climate simulations with low computational cost. Furthermore it enables us to isolate the individual effects of glacial ocean circulation, solubility and sea-ice coverage on atmospheric CO_2.

An earlier study has also attempted to evaluate the impact of individual climatic factors on the marine carbon cycle using idealized AMOC states (Cameron et al., 2005). We expand their approach by analyzing the atmospheric pCO_2 response to each factor of climate dynamics obtained from glacial AOGCM simulations.

CPD
7, 1261–1299, 2011

2 Method

2.1 AOGCM and an offline biogeochemical model

We used an ocean biogeochemical model with an offline tracer advection scheme (Oka et al., 2008, 2011). A homogenized box atmosphere is coupled to a three-dimensional ocean biogeochemical model. In the tracer calculations, the model uses prescribed monthly climatology from 30-yr averages of horizontal ocean velocities, vertical diffusivity, sea surface height, sea surface wind speed, sea ice fraction, and sea-surface solar radiation, derived from a series of AOGCM experiments conducted with the Model for Interdisciplinary Research on Climate (MIROC) version 3.2 (K-1 model developers, 2004). These boundary conditions are interpolated from the $1.4^{\circ} \times 0.9^{\circ}$ averaged resolution of MIROC to 2.8° latitude $\times$ 2.8° longitude grids for the biogeochemical model to reduce computational cost (Oka et al., 2011). Meridional and zonal velocities are interpolated while preserving water volume flux at each grid. The other boundary conditions are linearly interpolated to the biogeochemical model grids. There are 44 vertical levels, which is the same resolution as that of MIROC.

The biogeochemical model is based on a simplified ecosystem of nutrient-phytoplankton-zooplankton-detritus (NPZD) ecosystem model (Plattner et al., 2001). The model includes two plankton functional groups of phytoplankton and zooplankton, suspended and sinking particulate detritus, four dissolved inorganic components of alkalinity, dissolved inorganic carbon (DIC), nitrate, and oxygen, and two carbon isotopes (^{13}C and ^{14}C). Biological production of particulate organic carbon (POC) depends on the available nitrate concentration and insolation based on Michaelis-Menten kinetics. The detritus sinking rate is $8\,m\,day^{-1}$ and the remineralization rate is $0.1\,day^{-1}$ above 100 m and $0.02\,day^{-1}$ below 100 m depth (Plattner et al., 2001). The production rate of calcium carbonate ($CaCO_3$) is assumed to be proportional to that of POC ($CaCO_3$:POC = 0.08) and the settling flux of particulate $CaCO_3$ in the water column decreases with an e-folding depth of 3500 m (Yamanaka and Tajika, 1996). The air-sea gas exchange of CO_2 is parameterized with a wind-speed dependent gas

CPD
7, 1261–1299, 2011

transfer coefficient (Wanninkhof, 1992). The oxygen gas exchange is determined by the temperature-dependent saturation state with respect to dissolved oxygen at the sea surface (Keeling et al., 1998). Atmospheric $\delta^{13}C$ and $\Delta^{14}C$ are set to −6.5 and 0, respectively.

2.2 Experimental design

In this study, two pairs of preindustrial and glacial AOGCM simulations are used. The first set of preindustrial (PIa) and LGM (LGa) simulations contributed to PMIP2 intercomparison (Yanase and Abe-Ouchi, 2007; Otto-Bliesner et al., 2007). In the second pair of preindustrial (PIb) and LGM (LGb) experiments, we have applied a form of flux adjustment in order to reduce a warm bias around Antarctica, as seen in the PMIP2 simulations. Added to the normal calculated heat flux is heat flux anomaly with a cooling tendency which is latitudinally dependent and varies from $0\,W\,m^{-2}$ at 45° S to $-15\,W\,m^{-2}$ at 80° S. In addition, an isopycnal/Gent-McWilliams (GM) eddy parameterization that parameterizes mesoscale eddy mixing on isopycnal surfaces (Gent and McWilliams, 1990) was changed to 7.0×10^{-6} instead of 3.0×10^{-6} in the PIa and LGa versions. Both pairs of preindustrial and glacial experiments were conducted with the PMIP2 experimental protocol (Braconnot et al., 2007) with respect to continental ice sheet conditions (Peltier, 2004), tracer gases, and Earth's orbital parameters (Berger, 1978). The AOGCM climatologies that are applied to the offline carbon cycle experiments are based on the last 30 yr of the MIROC 3.2 PIa, PIb, LGa, and LGb simulations.

To mimic the effects of enhanced AABW formation on the marine carbon system under preindustrial conditions, we use the PIb climatology that is based on the last 30 yr of a 2019-yr-long integration under 1850 AD conditions. The additional surface heat flux forcing was applied after 1800 yr of the total integration. For LGb, the climatology from the last 30 yr of a 3029-yr integration under LGM condition is used. The additional heat flux forcing that leads to an enhancement of AABW formation was applied after 2700 yr of LGM integration. In all cases, we assume climatology as a steady-state system by repeating monthly climate conditions as forcing for the carbon cycle model.

CPD
7, 1261–1299, 2011

The ocean carbon cycle simulations for both preindustrial experiments are spun up for 10 000 yr with prescribed atmospheric pCO_2 of 280 ppm so that the solution can reach equilibrium in the atmospheric and oceanic carbon cycling. After 10 000 yr of integration, we prognosticate the preindustrial marine carbon cycle and atmospheric pCO_2 variations. The carbon stored in the ocean reservoir amounts to 39 200 and 39 600 GtC in PIa and PIb, respectively. The glacial simulations LGa, LGb of the marine carbon cycle are run for 5000 yr starting from the equilibrated states of the preindustrial ocean carbon cycle experiments PIa, PIb, respectively. We analyze the response of the carbon cycle to the different physical forcings derived from the MIROC experiments.

2.3 Setup of factorial experiments

Idealized factorial model experiments are performed with the off-line carbon cycle model to separate the sensitivity of atmospheric pCO_2 with respect to changes in solubility, ocean circulation, and sea-ice coverage in both Northern and Southern Hemispheres (Table 1). Experiment LGa-sl is identical to LGa, except that it uses the preindustrial SST, sea surface salinity (SSS), and wind speed. In this case, the wind speed is used only for determining the air-sea gas exchange. This experiment evaluates the anomalous solubility-induced pCO_2 fluxes into the atmosphere. Experiment LGa-in is similar to LGa, except that it uses the preindustrial sea-ice fraction and insolation in the Northern Hemisphere only. Note that this factorial experiment (LGa-in) isolates the effects of gas exchange and biological production due to sea-ice coverage, but does not include the ocean circulation change induced by the sea ice extent. The experiment focuses on the influence of the Northern Hemisphere sea ice on the ocean carbon cycle. Correspondingly, experiment LGa-is is obtained by modifying LGa to use the preindustrial Southern Hemisphere sea-ice fraction and insolation, and it is conducted to estimate the atmospheric pCO_2 response to the glacial sea ice in the Southern Ocean. Experiment LGa-oc is based on LGa, but it uses the preindustrial topography, ocean vertical and horizontal velocities, sea surface height, vertical diffusivity, and oceanic interior temperature and salinity. This experiment can isolate the atmospheric

CPD
7, 1261–1299, 2011

pCO_2 sensitivity to the glacial ocean circulation. In the offline biogeochemical model, the isopycnal surfaces are recalculated using the temperature and salinity in the ocean interior, which affect the isopycnal mixing of tracers. Interior temperature and salinity fields are therefore applied only for tracer mixing along the isopycnal surface. All factorial experiments except for LGa-oc use the glacial topography. These factorial experiments are run for 2000 yr, and they correspond to switching off individual glacial climatic factors. In the following we assess the carbon cycle differences between LGa (full glacial experiment) and each factorial experiment (Table 2).

In order to investigate the effects of glacial salinity, temperatures and wind speed on the CO_2 solubility, we conduct a second set of factorial experiments under preindustrial climate conditions (Table 1). Experiment PIa-sl is similar to the preindustrial experiments of PIa, but uses glacial SST, SSS and wind speed in the air-sea gas exchange parameterization. This experiment focuses on the glacial solubility effect in an interglacial environment. Experiment PIa-in is based on the PIa experiment but uses the glacial sea-ice concentration and insolation in the Northern Hemisphere. Similarly, experiment PIa-is is obtained from PIa, except that it uses the glacial sea-ice concentration and insolation in the Southern Hemisphere. These two experiments will help to quantify the atmospheric pCO_2 sensitivity to interglacial/glacial changes in sea-ice coverage and solar insolation in the Northern and Southern Hemispheres. Experiment PIa-oc is obtained from the preindustrial experiments, PIa, except that it uses the glacial topography, ocean vertical and horizontal velocities, sea surface height, vertical diffusivity, and oceanic interior temperature and salinity. This experiment isolates the atmospheric pCO_2 response to the glacial ocean circulation under preindustrial boundary conditions. In the second set of experiments, all experiments use glacial sea surface area as topography. In these experiments, the topography change is considered to reflect the expanded ice sheet, which affects the total ocean surface area of air-sea interaction. The second set of factorial experiments corresponds to switching on the glacial climate factors under the modern background climate state. The contributions of glacial solubility, ocean circulation, and sea ice in both hemispheres

CPD
7, 1261–1299, 2011

to atmospheric pCO_2 are estimated by the atmospheric pCO_2 difference from PIa in each factorial experiment (Table 2). Factorial experiments of LGb simulation are also conducted, as well as factorial experiments of LGa. Comparison between results of the first and second factorial experiments allows us to evaluate the ocean carbon cycle dependence on the background state of climate.

3 Preindustrial and glacial marine carbon cycle simulations

3.1 Validation of present ocean carbon cycle simulation

The results of PIa and PIb are shown in Fig. 1. In both cases, the surface nitrate concentration is high in the Southern Ocean and the North Pacific (Fig. 1b and c), in accordance with observational data (Levitus et al., 1994) (Fig. 1a). The surface nutrient concentrations are underestimated in the eastern equatorial Pacific in both cases. This can be explained by the fact that we set the vertical velocity of particulate detritus lower than that of Plattner et al. (2001); the slower settling particulates contribute to the POC regeneration at the depths below the euphotic zone. This brings nutrient out of the euphotic layer, thereby decreasing the nutrient concentration at the surface (Fig. 1b and c). The excess nitrate off the coast of Chile and in the Atlantic sector of the Southern Ocean is attributable to the deep-water supply via coastal upwelling or convective mixing.

Our model does not consider temperature-dependent biological production (Oschlies and Garcon, 1999). Consequently, SST in the Southern Ocean less affects the nitrate distribution. Rather, it reflects the ocean circulation state and upwelling regions, with some sensitivity to the isopycnal/GM mixing parameterization.

The net primary production fluxes are 68.6 GtC yr^{-1} in PIa and 59.5 GtC yr^{-1} in PIb. These fluxes are larger than a recent satellite based estimate (48 GtC yr^{-1}, in Behrenfeld et al., 2006). The export fluxes of particulate organic matter of 10.5 and 10.4 GtC yr^{-1} in PIa and PIb (Fig. 1e and f) are in line with observationally-based

CPD
7, 1261–1299, 2011

estimates of 5–20 GtC yr^{-1} (Jahnke and Jahnke, 2004; Falkowski et al., 1998; Laws et al., 2000; Louanchi and Najjar, 2000).

The values of deep-water $\Delta^{14}C$ in the North Pacific reach −206 and −222 per mil in PIa and PIb (Fig. 1h and i), respectively. These values are within the range of the regionally averaged value of −214 per mil from observational pre-bomb measurements (Key et al., 2004) (Fig. 1g). The values of deep-water $\Delta^{14}C$ in the North Pacific Ocean and the Southern Ocean in PIb are smaller than the observational estimates. We attribute this to a lower radiocarbon value at the Southern Ocean surface in PIb compared with the observed radiocarbon data. This might be caused by the sea-ice coverage that decreases the sea surface radiocarbon values by preventing air-sea gas exchange of radiocarbon between atmosphere and ocean.

We estimate the preformed nutrient concentration indicating water-mass transport by ocean circulation as a conservative water-mass tracer (Ito and Follows, 2005). We simulate nitrate cycling of the ocean, but neglect denitrification and N_2 fixation processes. Therefore, the nitrate total inventory does not change in our model from Levitus World Ocean atlas (Levitus et al., 1994). The nitrate concentration corresponds linearly to phosphate concentration in our model. When we estimate phosphate concentration from nitrate concentration, we use a constant N:P stoichiometry (R_{NP}) of 14.21 based on the ratio of nitrate to phosphate in Levitus data. The preformed phosphate ($[PO_4]^*$) is calculated following Broecker et al. (1999b) as

$$[PO_4]^* = ([NO_3] - [AOU] \times R_{NO}) \times R_{NP}. \quad (1)$$

Here, $[NO_3]$ is the nitrate concentration, [AOU] is the utilized oxygen concentration ($[O_2]_{sat}$-$[O_2]$), and R_{NO} is a constant N:O_2 stoichiometry in our model (set to 8.526). The global-mean preformed phosphate concentrations are 1.05 and 0.75 µmol kg^{-1} in PIa and PIb, and the fractions of preformed phosphate to the global mean phosphate concentration (2.06 µmol kg^{-1}) are 0.50 and 0.36 in PIa and PIb, respectively. The value in PIa is close to the estimate of 0.51 from Levitus data. This means that the ocean fills with a nearly uniform mixture of deep water below 1500 m produced in the

CPD
7, 1261–1299, 2011

Northern Atlantic and the Southern Ocean. The preindustrial condition in PIb, on the other hand, shows that deep waters are more produced in the North Atlantic rather than in the Southern Ocean. From these results it becomes apparent that under preindustrial conditions the simulated distribution of biogeochemical tracers is sensitive to the heat flux forcing applied to the ocean and the GM parameterization.

3.2 Glacial climate simulations and the ocean carbon cycle

Whereas LGa shows an enhanced North Atlantic Deep Water (NADW) formation under the glacial conditions (Fig. 2a and b), LGb exhibits an intensified AABW formation in association with the shoaling of NADW (Fig. 2c and d). The maximum of NADW flow is 25.8 Sv and 8.2 Sv in LGa and LGb, respectively and the minimum of AABW flow is 4.5 Sv and 8.5 Sv in LGa and LGb, respectively. The resulting change in poleward heat transport in MIROC associated with the AMOC changes affects the SST and sea-ice extent in both hemispheres (Fig. 3a and b). Southern Ocean and North Atlantic sea ice are found at lower latitudes in LGb than in LGa. Compared to PIa and PIb, the average temperatures of Southern Ocean deep waters lower by 0.9 and 1.5 °C in LGa and LGb (Fig. 4a and c), respectively, and both reach levels near freezing point. In the tropical Atlantic, the bottom temperature in LGb decreases by 3.5 °C, corresponding to the oxygen isotope based reconstruction of deep water temperature during the last glacial maximum (Schrag et al., 1996). The average salinity increases in both cases (Fig. 4b and d), reflecting the change in sea-level applied to MIROC in LGa and LGb. We see in particular a large increase in salinity in AABW as a result of strong brine rejection in the Southern Ocean. The averaged potential density of the Southern Ocean deep water increases by 0.19 $kg\,m^{-3}$ in LGa and 0.29 $kg\,m^{-3}$ in LGb, which is associated with colder temperature and higher salinity. Compared to LGa, AABW covers a larger volume in LGb. The simulated Southern Ocean sea ice in LGb is comparable to the observational data of September sea-ice distribution (Gersonde et al., 2005). On the other hand, the sea ice-covered area in the North Atlantic extends

CPD
7, 1261–1299, 2011

down to 40° N in LGb, which is an overestimation in comparison with sea-ice proxy data (Sarnthein et al., 2003).

Associated with the enhanced NADW formation in LGa, DIC decreases by 32 mmol m^{-3} in the Atlantic deep water and increases by 28 mmol m^{-3} in the intermediate North Pacific water (Fig. 5a and b). The changes in carbon inventory are −10.4 GtC in the Atlantic, −1.4 GtC in the Southern, and +5.9 GtC in the Pacific Oceans. This suggests that the intensified NADW results in delivering DIC from Atlantic to Pacific basins in association with an enhanced Atlantic meridional circulation. On the other hand, LGb represented by a weakened NADW and an increased AABW reduces DIC by 32 mmol m^{-3} in the subsurface and increases by 17 mmol m^{-3} in the deep Atlantic Ocean (Fig. 5c). The carbon inventories are reduced among the three basins. The increase in vertical DIC gradient between the surface and deep water indicates the more effective storage of carbon in the abyssal ocean in LGb. This response is also present in the North Pacific Ocean (Fig. 5d).

Simulated changes in the overturning circulation affect also the nutrient distribution. The enhanced NADW formation in LGa increases the euphotic nitrate concentration in the North Atlantic Ocean (Fig. 6a). This means that the vigorous deep convection supplies nutrient-rich deep water to the surface. The increasing surface nutrient concentrations also appear in upwelling regions, such as the equatorial eastern Pacific and the western North Pacific Oceans. Along the sea ice margin, nutrient supplies from the sea ice area (Fig. 6a) and biological production thus increases in the marginal sea ice zone (Fig. 6b). Biological production weakens under the sea ice region because the expanded sea ice prevents insolation from reaching the ocean surface. Export flux of POC reduces by only −1.5%. The oceanic carbon uptake is changed, as shown by the large anomalous air-sea CO_2 flux at high latitudes (Fig. 6c).

In LGb, the reduced ventilation associated with the weakening of NADW formation weakens the transport of nutrient-rich deep waters to the surface and reduces surface nitrate concentrations (Fig. 6d). The surface nutrient reduction weakens biological productivity globally (Fig. 6e), and the export flux of POC is reduced by 1.7 GtC yr^{-1}. The

CPD
7, 1261–1299, 2011

lack of an iron cycle in our marine carbon cycle model likely accounts for the underestimation in biological production around Antarctica compared with paleoproxy data compilations (Bopp et al., 2003; Oka et al., 2011). The air-sea CO_2 flux increases over the regions of annual sea ice coverage (Fig. 6f), which leads to a release of CO_2 from mixing of DIC-rich water. On the other hand, the air-sea CO_2 flux reduces along the sea ice margin, thereby increasing the oceanic carbon uptake. The difference in responses of air-sea CO_2 gas exchange in the western North Pacific region of LGa and that of LGb may be affected by the deep-water circulation patterns that accompany carbon-rich water.

Glacial changes in biological conditions affect the ocean carbon uptake considerably. The fraction of global-mean preformed phosphate to the global-mean phosphate concentration decreases by 0.020 µmol kg^{-1} in LGa from the preindustrial condition, whereas it increases by 0.028 in LGb. The increase in preformed nutrient in LGb suggests that biological uptake of CO_2 weakens under the glacial climate conditions and the change in the efficiency of the biological pump would contribute rather to the atmospheric pCO_2 rise, than to a reduction. It should be noted, however, that the estimate of preformed nutrient concentrations is sensitive to the surface oxygen concentration at polar region, so that the comparison between the preindustrial and glacial states must be interpreted with caution.

4 The effects of glacial climate factors on atmospheric pCO_2

The atmospheric pCO_2 is lowered by only 23.7 ppm in LGa, while it is reduced by 20.0 ppm in LGb (Fig. 7). These values are much smaller than the observed glacial-interglacial pCO_2 difference of 90 ppm. This may either suggest that the carbon cycle model is missing important components or that the prescribed ocean changes from MIROC are not adequate to trigger a larger response in the carbon cycle. In this section we will try to disentangle the individual contributions to the glacial pCO_2 reduction and assess their uncertainties using a series of factorial sensitivity experiments

CPD
7, 1261–1299, 2011

(Tables 1 and 2). The sensitivities of atmospheric pCO_2 to gas solubility, ocean circulation, and sea-ice coverage in the Northern and Southern Hemispheres are summarized in Fig. 7. The pCO_2 responses to these individual climate factors are larger for LGb than for LGa because the marine carbon cycle appears to respond nonlinearly to a reorganization of ocean circulation in conjunction with large extent of sea ice. In addition, the total sums of all factorial pCO_2 changes are different for the preindustrial and glacial base, indicating potential background state dependence of these sensitivities and potentially of climate carbon cycle feedbacks. The total sum of the individual sensitivities are 26.7 ppm in LGa and 24.2 ppm in LGb, which is close to the LGa and LGb full experimental results that capture the combined effect of all forcings.

4.1 Solubility effect

The solubility change lowers atmospheric pCO_2 by 34.8 ppm in LGb-sl (Fig. 7). This change contributes most significantly to the full glacial pCO_2 lowering shown as the LGb result. The solubility effect on atmospheric pCO_2 simulated here is larger than the upper bound of previous estimates of −30 ppm according to intermediate complexity and GCM models (Kohfeld and Ridgwell, 2009), suggesting that our model overestimates the solubility effect. This is because we do not consider the weakening of the solubility pump due to the salinity increase of 1 psu. We estimate the effect of salinity on CO_2 solubility to result in a 10-ppm pCO_2 increase. This would bring the estimate of the combined solubility effect of temperature and salinity inside the range of previous estimates between −21 and −30 ppm (Kohfeld and Ridgwell, 2009).

The solubility changes under the glacial and preindustrial background conditions (i.e., LGb-sl and PIb-sl) are quite similar (stars and circles in Fig. 7). The DIC responses to the solubility change as well as pCO_2 changes are similar in LGb-sl and PIb-sl, although the amplitudes of DIC anomalies in LGb-sl and PIb-sl are slightly different (Fig. 8a and e). This suggests that the solubility is relatively independent of other climatic factors. The slightly smaller pCO_2 change in LGb-sl compared with that in PIb-sl could be related to the difference between sea ice coverage under glacial conditions

CPD
7, 1261–1299, 2011

and under preindustrial conditions. Since the expanded sea ice decreases the area of outcropping cold water, ocean carbon uptake is reduced at high-latitudes (Fig. 9a and e).

4.2 Sea ice coverage in the Northern Hemisphere

In LGb-in the expansion of glacial sea ice coverage in the Northern Hemisphere increases atmospheric pCO_2 (Fig. 7), because the sea ice in the northern North Atlantic prevents oceanic carbon uptake through gas solubility. The weakening of gas solubility in the northern area obviously reduces DIC of the whole Atlantic Ocean (Fig. 8b).

Similarly, the atmospheric pCO_2 increases in PIb-in. The large difference in DIC between LGb-in and PIb-in emerges at intermediate depths in the North Atlantic (Fig. 8b and f). The ocean circulation in PIb-in corresponds to vigorous preindustrial AMOC. Therefore, compared to LGb-in the intensified ocean circulation exports more carbon from the North Atlantic to the other oceans and hence reduces DIC over the North Atlantic Ocean (Fig. 8b and f). As a result, the increase in atmospheric pCO_2 is larger in PIb than in LGb. Our results support a previous study that argues that the North Atlantic plays a significant role in the global carbon uptake and the ocean carbon cycle (Kurahashi-Nakamura et al., 2010).

The sea ice cover weakens biological production, because it reduces the penetration of solar irradiance into the ocean. Contrasting this effect, biological production increases along the sea-ice margin as unutilized nutrients are supplied to the open ocean. Consequently, biological production does not change atmospheric pCO_2 considerably.

4.3 Sea ice coverage in the Southern Hemisphere

Compared with the sea-ice coverage in the Northern Hemisphere, the glacial sea ice in the Southern Hemisphere reduces atmospheric pCO_2 by 6.2 ppm (Fig. 7). The sea-ice coverage extends over the upwelling region of the Southern Ocean, and the air-sea

CPD
7, 1261–1299, 2011

gas exchange close to Antarctica is decreased (Fig. 9c). This result suggests that the sea ice change in the Southern Ocean inhibits CO_2 release into the atmosphere, but to a lesser extent than proposed by Stephens and Keeling (2000).

Light limitation in the extended glacial perennial sea-ice region reduces biological production. In the marginal sea-ice zone, biological production in turn increases due to the nutrient supply from the permanent sea ice region resulting in a 4.2% decrease of export flux of POC. The pCO_2 lowering from inhibition of CO_2 degassing in the polar region partly counteracts the pCO_2 rise through the weakening of biological production. The opposing effects of physical and biological processes on atmospheric pCO_2 were also described in a recent coupled climate-carbon simulation study (Kurahashi-Nakamura et al., 2007).

4.4 Ocean circulation

Enhanced AABW formation in LGb increases the DIC storage in the abyssal ocean (Fig. 8d) and changes the oceanic carbon uptake around Antarctica (Fig. 9d). Despite these large-scale responses, the sensitivity of atmospheric pCO_2 to the glacial/interglacial ocean circulation changes is small in LGb-oc. To analyze the effect of ocean circulation on marine geochemistry, we examine the differences in the zonally-averaged ocean surface DIC (ΔDIC), alkalinity (ΔALK), pH (ΔpH), and CO_2 concentration (ΔCO_2) due to the imposed glacial-interglacial ocean circulation change (Fig. 10). In this study, the total oceanic-atmosphere carbon inventory is stable, as we neglect the global carbon budget change through sedimentation processes and changes in land weathering processes. This means that our estimate in this study is subject to the oceanic chemistry change induced only by climatic factors.

The weakening of NADW formation reduces ΔDIC and ΔALK significantly in the entire North Atlantic (Fig. 10a). In turn, ΔDIC and ΔALK increase south of 60° S because the upwelled carbon-rich deep waters stay below the sea ice area.

However, it should be noted that the glacial ocean circulation alters ΔDIC and ΔALK simultaneously in the Atlantic and Pacific basins (Fig. 10a and b). Therefore these

CPD
7, 1261–1299, 2011

changes cause only a small change in surface pH and thus reduce atmospheric pCO_2 only slightly (Fig. 10c and d). At high latitudes, the surface ocean ΔCO_2 increases substantially, but the increasing CO_2 is mostly not released into the atmosphere because of the sea ice coverage. A decrease in ΔDIC that was greater than that in ΔALK would increase pH and greatly reduce atmospheric pCO_2. The simulated small difference between ΔDIC and ΔALK in our glacial experiment consequently leads to a small reduction in atmospheric CO_2.

5 Discussion

5.1 Deep-water formation patterns and changes in carbon storage

The strength and structure of NADW formation are connected to the strength of AABW formation; the export of NADW into the Southern Ocean partly controls the vertical density structure in the AABW formation regions, which translates into changes of AABW production. Our LGb experiment exhibits a weakening of NADW formation and an increase in AABW volume under the glacial conditions. The weakening of NADW formation reduces northward heat transport in the Atlantic Ocean. The glacial ocean circulation seems to be determined by the balance between thermal buoyancy fluxes at northern high latitudes and haline buoyancy fluxes at southern high latitudes, as discussed by Gildor et al. (2002). However, the salinity increase of 1.7 psu in the Southern Ocean deep water is not enough to justify the glacial proxy data variability by 2.4 psu at a single deep-depth core of the Southern Ocean (Adkins et al., 2002). Although our analysis cannot distinguish between the haline and thermal effects on ocean circulation and resulting glacial-interglacial CO_2 changes, it is qualitatively supporting the notion that denser AABW will provide a means to sequester atmospheric CO_2 during glacial condition (Bouttes et al., 2010).

Our study shows a small sensitivity of atmospheric pCO_2 to glacial-interglacial ocean circulation changes, whereas a recent study with an earth system model of

CPD
7, 1261–1299, 2011

intermediate complexity (EMIC) documented a much larger sensitivity (Brovkin et al., 2007). A large difference between their and our study is found in the salinity change and the associated DIC increases south of 40° S. This supports again the idea that the pattern of stratification changes in the Northern and Southern Hemisphere plays a key role in controlling glacial pCO_2.

Furthermore, such differences could also be related to the fact that simplified two-dimensional ocean models, as used by Brovkin et al. (2007), can not resolve the full 3-dimensional structure of the ocean which may be important in the biogeochemical response to LGM climate change (Bouttes et al., 2009). Horizontal effects may affect the distribution of DIC at the surface. Also, the established Southern Ocean deep water formation in our model is substantially different from box model studies (Watson and Naveira Garabato, 2006; Paillard and Parrenin, 2004), which have argued that a large reduction in atmospheric pCO_2 results from enhanced stratification of the Southern Ocean. The box models tend to simulate a larger high-latitude sensitivity of pCO_2 to climate forcing compared with GCMs, because they have a larger outcropping area in the polar region (Bacastow, 1996; Archer et al., 2000; Broecker et al., 1999a).

Potential shifts in the source regions of deep-water from the North Atlantic to the Southern Ocean could change the strength of biological pump in the ocean. Toggweiler et al. (2003) argued that the increase in Southern Ocean deep-water formation weakens biological production through utilized nutrient redistribution, thereby changing the atmospheric pCO_2 response to the ocean circulation change. In LGb, the fraction of preformed nutrient to the total nutrient increases by a small factor of 0.028. Following the simplified estimate of the atmospheric pCO_2 change from the fraction change, the atmospheric pCO_2 change is +8.7 ppm due to biological efficiency. The reorganization of the Southern Ocean causes carbon storage and redistribution of nutrient, but these effects on the atmospheric pCO_2 tend to cancel out.

CPD
7, 1261–1299, 2011

5.2 Potential of ocean biogeochemical effects on atmospheric pCO_2

The glacial ocean circulation drives DIC and alkalinity anomalies simultaneously (Fig. 10), leading to a relatively small reduction in surface pH and ocean surface pCO_2. The marked reduction in NADW formation accounts for only a small reduction in surface pH (Fig. 10), because our simulation assumes a stable total carbon budget in the atmosphere and ocean systems as a closed system (Sigman et al., 1998). If we consider the variability in total carbon budget as a result of sedimentation process changes, atmospheric pCO_2 can change largely through variability in oceanic carbon and alkalinity inventories (e.g., Chikamoto et al., 2009). For example, when the deep water stores large quantities of carbon and becomes more acidic under glacial ocean circulation conditions (Brovkin et al., 2007) or when the AMOC collapses (Chikamoto et al., 2008), atmospheric pCO_2 further decreases due to carbonate compensation. Our glacial experiment also shows that stagnant deep water increases DIC and causes acidification of the overlying bottom water (not shown). This condition would potentially drive pH largely through carbonate compensation and the associated pCO_2 reduction.

The simultaneous changes in our simulation might also be influenced by the simplified biogeochemistry whereby the model assumes a constant export rain ratio and settling rate of particles everywhere. The export rain ratio of $CaCO_3$ to POC would be decoupled if the calcification rate of calcifying organisms is affected by seawater temperature. Calcification decreases in cold seawater environment below 10 °C (Maier-Reimer and Bacastow, 1990). A model simulation shows that the glacial SST conditions reduce calcification although the effect is limited to a small polar region (Brovkin et al., 2007). The remineralization of detritus is also sensitive to water temperature. When water temperature is lowered by 5 °C during glacial periods, remineralization decreases, thereby increasing carbon transport to the deep ocean and reducing atmospheric pCO_2 (Matsumoto, 2007). Furthermore, the shift in marine biota through a nutrient redistribution may effectively cause the decoupling of surface DIC and alkalinity changes. The change in marine biota species from coccoliths to diatoms would

CPD
7, 1261–1299, 2011

increase the surface alkalinity, which is further amplified when decreasing deposition of calcite dictates the total budget of the ocean through carbonate compensation. In this case, atmospheric pCO_2 reduces. The climate-induced biogeochemical processes would further amplify the atmospheric pCO_2 change.

5.3 Glacial westerlies

Anderson et al. (2009) proposed that possible glacial shifts of southern hemispheric westerlies may affect the strength and position of upwelling around Antarctica. Moreover, this shift as inferred from changes in biogenic silica during the last glacial termination correlates well with the timing of the atmospheric pCO_2 rise. However, quantification of this effect for highly idealized wind configurations using an earth system model yields only very small changes of atmospheric pCO_2 of roughly 5 ppm (Menviel et al., 2008). In the MIROC experiments LGa and LGb, the Southern Ocean westerly winds weaken slightly over the sea ice area, but their position remains virtually unchanged. The simulated small westerly change under glacial conditions agrees well with other coupled AOGCM simulations in PMIP2 (Rojas et al., 2009). When estimating only the effect of the wind speed change on atmospheric pCO_2, we find that a small change in the westerlies does not regulate atmospheric pCO_2 much. It should be noted that our simplified estimate considers only the wind-speed change in governing gas solubility and not the ocean circulation change induced by wind shift.

6 Conclusions

A series of sensitivity experiments with a marine carbon cycle model forced by different glacial/interglacial climate scenarios is conducted to quantify the effects of climate dynamical changes on atmospheric CO_2 concentration. Our study extends previous studies using either box models (Köhler et al., 2005) or intermediate complexity models (Brovkin et al., 2007) in that it is based on fully coupled AOGCM results and an offline marine carbon cycle model.

CPD
7, 1261–1299, 2011

In our glacial simulations, atmospheric pCO_2 decreases mainly due to an enhancement of gas solubility through lowering SST. Despite large differences of the MOC in two different LGM experiments neither a weakening of NADW nor an increase of AABW formation causes a large change in atmospheric pCO_2. Enhanced of AABW formation is obviously required to maintain the vertical gradient of DIC and causes deep water carbon sequestration in an isolated abyssal reservoir. However, the modest ocean stratification in the Southern Ocean may affect the availability of carbon storage in the abyssal ocean. The DIC storage causes acidification of the bottom waters, thereby decreasing calcite burial in sediments. This process would have an additional potential to affect the carbon budget change through carbonate compensation over thousands of years. This process has not been resolved in our experiments.

The sea-ice extent plays different roles in modulating atmospheric pCO_2 in two hemispheres. In the Northern Hemisphere, the sea-ice coverage increases atmospheric pCO_2 through less soluble CO_2, whereas the coverage in the Southern Ocean decreases the pCO_2 by inhibiting the degassing of DIC-rich deep water. This result adds another level of complexity to sea-ice-CO_2 feedbacks previous proposed Stephens and Keeling (2000).

Atmospheric pCO_2 is relatively insensitive to glacial ocean circulation as found in previous studies (Bopp et al., 2003; Tagliabue et al., 2009). In this study, the glacial ocean circulation causes simultaneous changes in surface DIC and alkalinity. These changes result in only a small pH change at the sea surface and a reduction in the availability of ocean carbon uptake. The simultaneous changes might be due to the simplified biogeochemistry whereby the model assumes constant export rain ratio and settling rate of particles everywhere. The water temperature dependence of decomposition (Matsumoto, 2007) and calcification rate (Maier-Reimer and Bacastow, 1990) may add new sensitivities to the marine carbon cycle's response to LGM climate change that need to be further assessed in future work.

CPD
7, 1261–1299, 2011

References

Adkins, J. F., Mcintyre, K., and Schrag, D. P.: The salinity, temperature, and $\delta^{18}O$ of the glacial deep ocean, Science, 298, 1769–1773, 2002. 1263, 1277

Anderson, R. F., Ali, S., Bradtmiller, L. I., Nielsen, S. H. H., Fleisher, M. Q., Anderson, B. E., and Bruuckle, L. H.: Wind-driven upwelling in the Southern Ocean and the deglacial rise in atmospheric CO_2, Science, 323, 1443–1448, 2009. 1280

Archer, D., Winguth, A., Lea, D., and Mahowald, N.: What caused the glacial/interglacial atmospheric pCO_2 cycles?, Rev. Geophys., 38, 159–189, 2000. 1262, 1278

Archer, D., Martin, P. A., Milovich, J., Brovkin, V., Plattner, G., and Ashendel, C.: Model sensitivity in the effect of Antarctic sea ice and stratification on atmospheric pCO_2, Paleoceanography, 18, 1012–1017, 2003. 1264

Bacastow, R. B.: The effect of temperature change on the warm surface waters of the oceans on atmospheric CO_2, Glob. Biogeochem. Cy., 10, 319–333, 1996. 1278

Bacastow, R. and Maier-Reimer, E.: Ocean-circulation model of the carbon cycle, Clim. Dynam., 4, 95–125, 1990. 1263

Behrenfeld, M. J. and Falkowski, P. G.: Photosynthetic rates derived from satellite-based chlorophyll concentration, Limnol. Oceanogr., 42, 1–20, 1997. 1290

Behrenfeld, M. J., O'Malley, R. T., Siegel, D. A., McClain, C. R., Sarmiento, J. L., Feldman, G. C., Milligan, A. J., Falkowski, P. G., Letelier, R. M., and Boss, E. S.: Climate-driven trends in contemporary ocean productivity, Nature, 444, 752–755, 2006. 1269

Berger, A.: Long-term variations of caloric insolation resulting from the earth's orbital elements, Quatern. Res., 9, 139–167, 1978. 1266

Bopp, L., Kohfeld, K. E., and Quéré, C. L.: Dust impact on marine biota and atmospheric CO_2 during glacial periods, Paleoceanography, 18, 1046, doi:10.1029/2002PA000810, 2003. 1273, 1281

Bouttes, N., Roche, D. M., and Paillard, D.: Impact of strong deep ocean stratification on the glacial carbon cycle, Paleoceanography, 24, PA3203, doi:10.1029/2008PA001707, 2009. 1278

Bouttes, N., Paillard, D., and Roche, D. M.: Impact of brine-induced stratification on the glacial carbon cycle, Clim. Past, 6, 575–589, doi:10.5194/cp-6-575-2010, 2010. 1263, 1277

Bouttes, N., Paillard, D., Roche, D. M., Brovkin, V., and Bopp, L.: Last Glacial Maximum CO_2 and $\delta^{13}C$ successfully reconciled, Geophys. Res. Lett., 38, L02705,

CPD
7, 1261–1299, 2011

doi:10.1029/2010GL044499, 2011. 1263
Braconnot, P., Otto-Bliesner, B., Harrison, S., Joussaume, S., Peterchmitt, J.-Y., Abe-Ouchi, A., Crucifix, M., Driesschaert, E., Fichefet, Th., Hewitt, C. D., Kageyama, M., Kitoh, A., Laîné, A., Loutre, M.-F., Marti, O., Merkel, U., Ramstein, G., Valdes, P., Weber, S. L., Yu, Y., and Zhao, Y.: Results of PMIP2 coupled simulations of the Mid-Holocene and Last Glacial Maximum - Part 1: experiments and large-scale features, Clim. Past, 3, 261–277, doi:10.5194/cp-3-261-2007, 2007. 1266
Broecker, W. S., Lynch-Stieglitz, J., Archer, D., Hofmann, M., Maire-Reimer, E., Marchal, O., Stocker, T., and Gruber, N.: How strong is the Harvardton-Bear constraint?, Glob. Biogeochem. Cy., 13, 871–820, 1999a. 1278
Broecker, W. S., Sutherland, S., and Peng, T.-H.: A possible 20th-Century slowdown of Southern Ocean deep water formation, Science, 286, 1132–1135, 1999b. 1270
Brovkin, V., Ganopolski, A., Archer, D., and Rahmstorf, S.: Lowering of glacial atmospheric CO_2 in response to changes in oceanic circulation and marine biogeochemistry, Paleoceanography, 22, PA4202, doi:10.1029/2006PA001380, 2007. 1264, 1278, 1279, 1280
Cameron, D. R., Lenton, T. M., Ridgwell, A. J., Shepherd, J. G., Marsh, R., and Yool, A.: A factorial analysis of the marine carbon cycle and ocean circulation controls on atmospheric CO_2, Glob. Biogeochem. Cy., 19, GB4027, doi:10.1029/2005GB002489, 2005. 1264
Chikamoto, M. O., Matsumoto, K., and Ridgwell, A.: Response of deep-sea $CaCO_3$ sedimentation to Atlantic meridional overturning circulation shutdown, J. Geophys. Res., 113, G03017, doi:10.1029/2007JG000669, 2008. 1279
Chikamoto, M. O., Matsumoto, K., and Yamanaka, Y.: Influence of Export rain ratio changes on atmospheric CO_2 and sedimentary calcite preservation, J. Oceanogr., 65, 209–221, 2009. 1279
Crowley, T. J.: Ice age terrestrial carbon changes revisited, Glob. Biogeochem. Cy., 9, 377–389, 1995. 1262
de Vernal, A., Rosell-Melé, A., Kucera, M., Hillaire-Marcel, C., Eynaud, F., Weinelt, M., Dokken, T., and Kagetama, M.: Comparing proxies for the reconstruction of LGM sea-surface conditions in the northern North Atlantic, Quat. Sci. Rev., 2525, 2820–2834, 2006. 1264
Dunne, J. P., Armstrong, R. A., Gananadesikan, A., and Sarmiento, J. L.: Empirical and mechanistic models for the particle export ratio, Glob. Biogeochem. Cy., 19, GB4026, doi:10.1029/2004GB002390, 2005. 1290
Falkowski, P. G., Barber, R. T., and Smetacek, V.: Biogeochemical Controls and Feedbacks on

CPD
7, 1261–1299, 2011

Ocean Primary Production, Science, 281, 200–206, 1998. 1270
Gent, P. and McWilliams, J. C.: Isopycnal mixing in ocean circulation models, J. Phys. Oceanogr., 20, 150–155, 1990. 1266
Gersonde, R., Crosta, X., Abelmann, A., and Armand, L.: Sea-surface temperature and sea-ice distribution of the Southern Ocean at the EPILOG Last Glacial Maximum – a circum-Antarctic view based on siliceous microfossil records, Quat. Sci. Rev., 24, 869–896, 2005. 1271
Gildor, H., Tziperman, W., and Toggweiler, J. R.: Sea ice switch mechanism and glacial-interglacial CO_2 variability, Glob. Biogeochem. Cy., 16, 1032, doi:10.1029/2001GB001446, 2002. 1263, 1277
Ito, T. and Follows, M. J.: Preformed phosphate, soft tissue pump and atmospheric CO_2, J. Mar. Res., 63, 813–839, 2005. 1263, 1270
Jahnke, R. A. and Jahnke, D. B.: Calcium carbonate dissolution in deep sea sediments: Reconciling microelectrode, pore water and benthic flux chamber results, Geochimica et Cosmochimica Acta, 68, 47–59, 2004. 1270
K-1 model developers: K-1 Coupled GCM (MIROC) Description, K-1 Technical Report No.1, edited by: Hasumi, H. and Emori, S., K-1 Technical Report, 1, 34 pp., 2004. 1265
Keeling, R. F., Stephens, B. B., Najjar, R. G., Doney, S. C., Archer, D., and Heimann, M.: Seasonal variations in the atmospheric O_2/N_2 ratio in relation to the kinetics of air-sea gas exchange, Glob. Biogeochem. Cy., 12, 141–163, 1998. 1266
Key, R. M., Kozyr, A., Sabine, L., Lee, K., Wanninkhof, R., Bullister, J. L., Feely, R. A., Millero, F. J., Mordy, C., and Peng, T.-H.: A global ocean carbon climatology: Results from Global Data Analysis Project (GLODAP), Glob. Biogeochem. Cy., 18, GB4031, doi:10.1029/2004GB002247, 2004. 1270, 1290
Kohfeld, K. E. and Ridgwell, A.: Glacial-interglacial variability in atmospheric CO_2, Surface Ocean/Lower Atmosphere Processes, Geophysical Monograph Series 37, Washington, DC, American Geophysical Union, 251–286, 2009. 1263, 1274
Köhler, P., Fischer, H., Munhoven, G., and Zeebe, R. E.: Quantitative interpretation of atmospheric carbon records over the last glacial termination, Glob. Biogeochem. Cy., 19, GB4020, doi:10.1029/2004GB002345, 2005. 1262, 1263, 1280
Kurahashi-Nakamura, T., Abe-Ouchi, A., Yamanaka, Y., and Misumi, K.: Compound effects of Antarctic sea ice on atmospheric pCO_2 change during glacial-interglacial cycle, Geophys. Res. Lett., 34, L20708, doi:10.1029/2007GL030898, 2007. 1264, 1276
Kurahashi-Nakamura, T., Abe-Ouchi, A., and Yamanaka, Y.: Effects of physical changes in the

CPD
7, 1261–1299, 2011

ocean on the atmospheric pCO_2: glacial-interglacial cycles, Clim. Dynam., 35, 713–719, doi:10.1007/s00382-009-0609-5, 2010. 1275
Laws, E. A., Falkowski, P. G., Smith Jr., W. O., Ducklow, H., and McCarthy, J. J.: Temperature effects on export production in the open ocean, Glob. Biogeochem. Cy., 14, 1231–1246, 2000. 1270
Levitus, S., Burgett, R., and Boyle, T.: World Ocean Atlas 1994 Volume 3: Nutrients, NOAA Atlas NESDIS 3, US Department of Commerce, Washington DC, 1994. 1269, 1270, 1290
Louanchi, F. and Najjar, R. G.: A global monthly climatology of phosphate, nitrate, and silicate in the upper ocean: Spring-summer export production and shallow remineralization, Glob. Biogeochem. Cy., 14, 957–977, 2000. 1270
Maier-Reimer, E. and Bacastow, R.: Modelling of geochemical tracers in the ocean, in: Climate-Ocean Interaction, edited by: Schlesinger, M. E., Kluwer Acad., Norwell, 233–267, 1990. 1279, 1281
Marinov, I., Gnanadesikan, A., Sarmiento, J. L., Toggweiler, J. R., Floows, M., and Mignone, B. K.: Impact of oceanic circulation on biological carbon storage in the ocean and atmospheric pCO_2, Glob. Biogeochem. Cy., 22, GB3007, doi:10.1029/2007GB002958, 2008. 1263
Matsumoto, K.: Biology-mediated temperature control on atmospheric pCO_2 and ocean biogeochemistry, Geophys. Res. Lett., 34, L20605, doi:10.1029/2007GL031301, 2007. 1279, 1281
Menviel, L., Timmermann, A., Mouchet, A., and Timm, O.: Climate and marine carbon cycle response to changes in the strength of the Southern Hemispheric westerlies, Paleoceanography, 23, PA4201, doi:10.1029/2008PA001604, 2008. 1280
Oka, A., Kato, S., and Hasumi, H.: Evaluating effect of ballast mineral on deep-ocean nutrient concentration by using an ocean general circulation model, Glob. Biogeochem. Cy., 22, GB3004, doi:10.1029/2007GB003067, 2008. 1265, 1290
Oka, A., Abe-Ouchi, A., Chikamoto, M. O., and Ide, T.: Mechanisms controlling export production at the LGM: effects of changes in oceanic physical field and atmospheric dust deposition, Glob. Biogeochem. Cy., doi:10.1029/2009GB003628, in press, 2011. 1265, 1273
Oschlies, A. and Garcon, V.: An eddy-permitting coupled physical-biological model of the North Atlantic 1. Sensitivity to advection numerics and mixed layer physics, Glob. Biogeochem. Cy., 13, 135–160, 1999. 1269
Otto-Bliesner, B. L., Hewitt, C. D., Marchitto, T. M., Brady, E., Abe-Ouchi, A., Crucifix, M.,

CPD
7, 1261–1299, 2011

Murakami, S., and Weber, S. L. .: Last glacial maximum ocean thermohaline circulation: PMIP2 model intercomparisons and data constraints, Geophys. Res. Lett., 34, L12706, doi:10.1029/2007GL029475, 2007. 1266
Paillard, D. and Parrenin, F.: The Antarctic ice sheet and the triggering of deglaciations, Earth Planet. Sci. Lett., 227, 263–271, 2004. 1278
Peacock, S., Lane, E., and Restrepo, J. M.: A possible sequence of events for the generalized glacial-interglacial cycle, Glob. Biogeochem. Cy., 20, GB2010, doi:10.1029/2005GB002448, 2006. 1263
Peltier, W. R.: Global glacial isostasy and the surface of the ice-age Earth: The ICE-5G (VM2) Model and GRACE, Ann. Rev. Earth Pl. Sc., 32, 111–149, 2004. 1266
Petit, J. R., Jouzel, J., Raynaud, D., Barkov, N. I., Barnola, J.-M., Basile, I., Bender, M., Chappellaz, J., Davis, M., Delaygue, G., Delmotte, M., Kotlyakov, V. M., Legrand, M., Lipenkov, V. Y., Lorius, C., Pépin, L., Ritz, C., Saltzman, E., and Stievenard, M.: Climate and atmospheric history of the past 420,000 years from the Vostok ice core, Antarctica, Nature, 399, 429–436, 1999. 1262
Plattner, G.-K., Joos, F., Stocker, T. F., and Marchal, O.: Feedback mechanisms and sensitivities of ocean carbon uptake under global warming, Tellus, 53B, 564–592, 2001. 1265, 1269
Rojas, M., Moreno, P., Kageyama, M., Crucific, M., Hewitt, C., Abe-Ouchi, A., Ohgaito, R., Brandy, E. C., and Hope, P.: The Southern westerlies during the last glacial maximum in PMIP2 simulations, Clim. Dynam., 32, 525–548, 2009. 1280
Sarnthein, M., Pflaumann, U., and Weinelt, M.: Past extent of sea ice in the northern North Atlantic inferred from foraminiferal paleotemperature estimates, Paleoceanography, 18, 1047, doi:10.1029/2002PA000771, 2003. 1272
Schrag, D. P., Hampt, G., and Murray, D. W.: Pore Fluid constraints on the temperature and oxygen isotopic composition of the glacial ocean, Science, 272, 1930–1932, 1996. 1271
Siegenthaler, U., Stocker, T. F., Monnin, E., Lüthi, D., Schwander, J., Stauffer, B., Raynaud, D., Barnola, J.-H., Fischer, H., Masson-Delmotte, V., and Jouzel, J.: Stable Carbon Cycle-Climate Relationship During the Late Pleistocene, Science, 310, 1313–1317, 2005. 1262
Sigman, D. M. and Boyle, E. A.: Glacial/interglacial variations in atmospheric carbon dioxide, Nature, 407, 859–869, 2000. 1262, 1263
Sigman, D. M., McCorkle, D. C., and Martin, W. R.: The calcite lysocline as a constraint on glacial/interglacial low-latitude production changes, Glob. Biogeochem. Cy., 12, 409–427, 1998. 1279

CPD
7, 1261–1299, 2011

Stephens, B. B. and Keeling, R. F.: The influence of Antarctic sea ice on glacial-interglacial CO_2 variations, Nature, 404, 171–174, 2000. 1264, 1276, 1281

Tagliabue, A., Bopp, L., Roche, D. M., Bouttes, N., Dutay, J.-C., Alkama, R., Kageyama, M., Michel, E., and Paillard, D.: Quantifying the roles of ocean circulation and biogeochemistry in governing ocean carbon-13 and atmospheric carbon dioxide at the last glacial maximum, Clim. Past, 5, 695–706, doi:10.5194/cp-5-695-2009, 2009. 1281

Toggweiler, J. R., Murnane, R., Carson, S., Gnanadesikan, A., and Sarmiento, J. L.: Representation of the carbon cycle in box models and GCMs 2. Organic pump, Glob. Biogeochem. Cy., 17, 1027, doi:10.1029/2001GB001841, 2003. 1278

Wanninkhof, R.: Relationship between wind speed and gas exchange over the ocean, J. Geophys. Res., 97, 7373–7382, 1992. 1266

Watson, A. J. and Naveira Garabato, A. C.: The role of Southern Ocean mixing and upwelling in glacial interglacial atmospheric CO_2 change, Tellus B, 58B, 73–87, 2006. 1263, 1278

Yamanaka, Y. and Tajika, E.: The role of the vertical fluxes of particulate organic matter and calcite in the oceanic carbon cycle: Studies using an ocean biogeochemical general circulation model, Glob. Biogeochem. Cy., 10, 361–382, 1996. 1265

Yanase, W. and Abe-Ouchi, A.: The LGM surface climate and atmospheric circulation over East Asia and the North Pacific in the PMIP2 coupled model simulations, Clim. Past, 3, 439–451, doi:10.5194/cp-3-439-2007, 2007. 1266

CPD
7, 1261–1299, 2011

Table 1. Factorial experimental design and results.

Simulations	pCO_2	Solubility	N sea ice	S sea ice	Circulation
LGa	256.3	LGa	LGa	LGa	LGa
LGa-sl	285.2	PIa	LGa	LGa	LGa
LGa-in	252.2	LGa	PIa	LGa	LGa
LGa-is	260.2	LGa	LGa	PIa	LGa
LGa-oc	256.2	LGa	LGa	LGa	PIa
PIa	280.0	PIa	PIa	PIa	PIa
PIa-sl	250.8	LGa	PIa	PIa	PIa
PIa-in	284.6	PIa	LGa	PIa	PIa
PIa-is	277.0	PIa	PIa	LGa	PIa
PIa-oc	282.6	PIa	PIa	PIa	LGa

Simulations	pCO_2	Solubility	N sea ice	S sea ice	Circulation
LGb	260.0	LGb	LGb	LGb	LGb
LGb-sl	294.8	PIb	LGb	LGb	LGb
LGb-in	252.1	LGb	PIb	LGb	LGb
LGb-is	266.2	LGb	LGb	PIb	LGb
LGb-oc	263.8	LGb	LGb	LGb	PIb
PIb	280.0	PIb	PIb	PIb	PIb
PIb-sl	242.1	LGb	PIb	PIb	PIb
PIb-in	296.5	PIb	LGb	PIb	PIb
PIb-is	282.7	PIb	PIb	LGb	PIb
PIb-oc	287.4	PIb	PIb	PIb	LGb

CPD
7, 1261–1299, 2011

Table 2. How the climate factor contributions to the ocean carbon cycle are estimated.

Contribution factors	Glacial base	Preindustrial base
Solubility	LGa – LGa-sl	PIa-sl – PIa
N sea ice	LGa – LGa-in	PIa-in – PIa
S sea ice	LGa – LGa-is	PIa-is – PIa
Ocean circulation	LGa – LGa-oc	PIa-oc – PIa
Solubility	LGb – LGb-sl	PIb-sl – PIb
N sea ice	LGb – LGb-in	PIb-in – PIb
S sea ice	LGb – LGb-is	PIb-is – PIb
Ocean circulation	LGb – LGb-oc	PIb-oc – PIb

CPD
7, 1261–1299, 2011

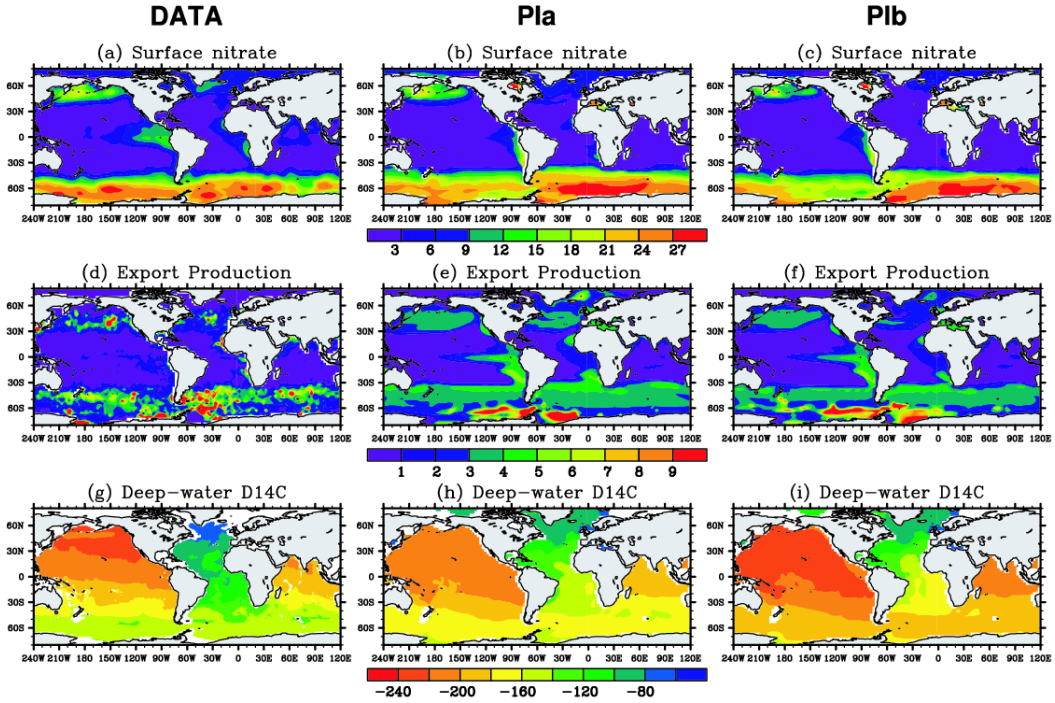

Fig. 1. Annual mean of nitrate concentration within the euphotic zone (mmol m^{-3}), export flux of POC (mmol m^{-2} yr^{-1}) and radiocarbon below 1500 m (per mil) for observational data (left panels), PIa (center), and PIb (right). Observational data refer to nitrate from Levitus World ocean atlas (Levitus et al., 1994). Export flux is estimated by Oka et al. (2008) based on the primary production algorithms (Behrenfeld and Falkowski, 1997) and the particle export ratios (Dunne et al., 2005). Natural radiocarbon data are taken from Global Ocean Data Analysis Project (Key et al., 2004).

CPD
7, 1261–1299, 2011

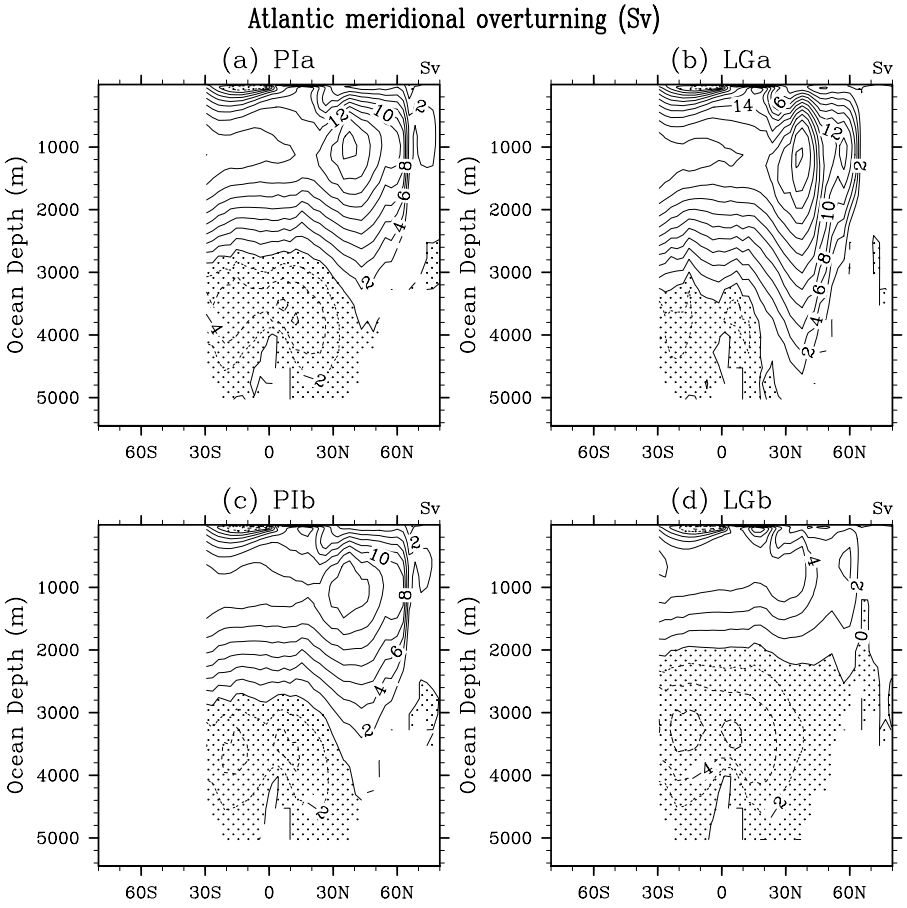

Fig. 2. Meridional overturning stream function (Sv) in the Atlantic Ocean of **(a)** PIa, **(b)** LGa, **(c)** PIb, and **(d)** LGb. Contour intervals are 2 Sv.

CPD
7, 1261–1299, 2011

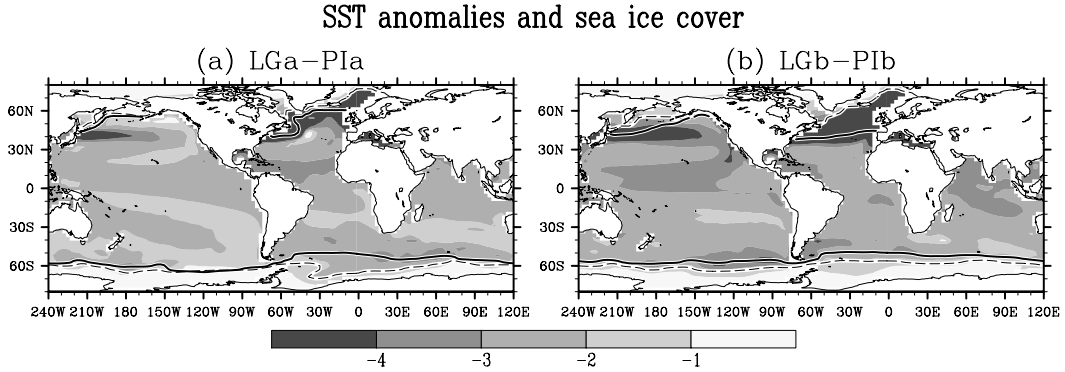

Fig. 3. SST anomaly **(a)** between LGa and PIa and **(b)** between LGb and PIb. Solid (dashed) lines show glacial (preindustrial) annual-mean sea ice fraction of 0.1.

CPD
7, 1261–1299, 2011

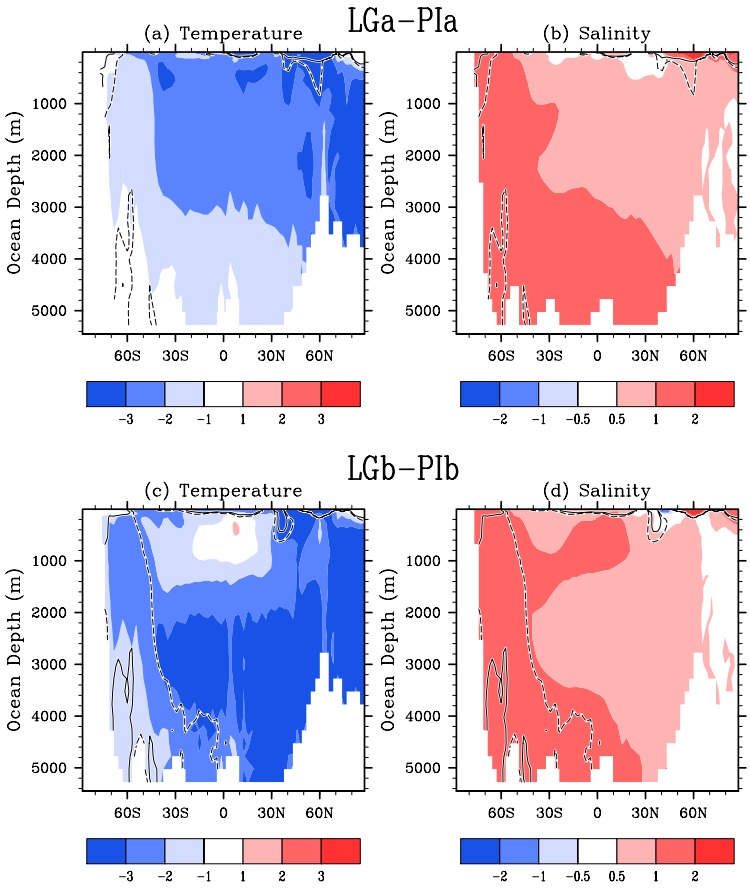

Fig. 4. Atlantic zonal-mean anomalies of potential temperature and salinity (**a** and **b**) between LGa and PIa and (**c** and **d**) between LGb and PIb. Salinity has been adjusted by 1 psu in each glacial AOGCM result to consider freshwater change due to frozen glacial ice sheets. Solid (dashed) lines indicate potential density anomaly of 0.35 (0.25) between each glacial and preindustrial simulations.

CPD
7, 1261–1299, 2011

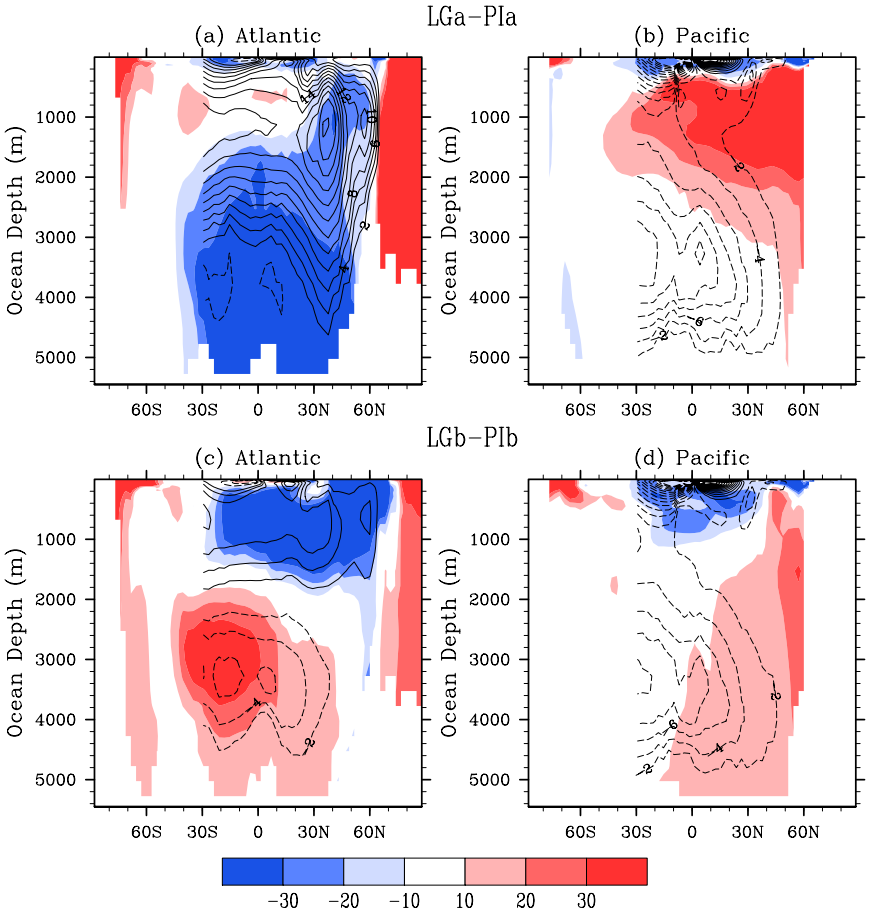

Fig. 5. Atlantic and Pacific DIC anomalies (mmol m^{-3}) (**a** and **b**) between LGa and Pla and (**c** and **d**) between LGb and Plb. Contour lines indicate the overturning stream function of each glacial simulation. Contour intervals are 2 Sv.

CPD
7, 1261–1299, 2011

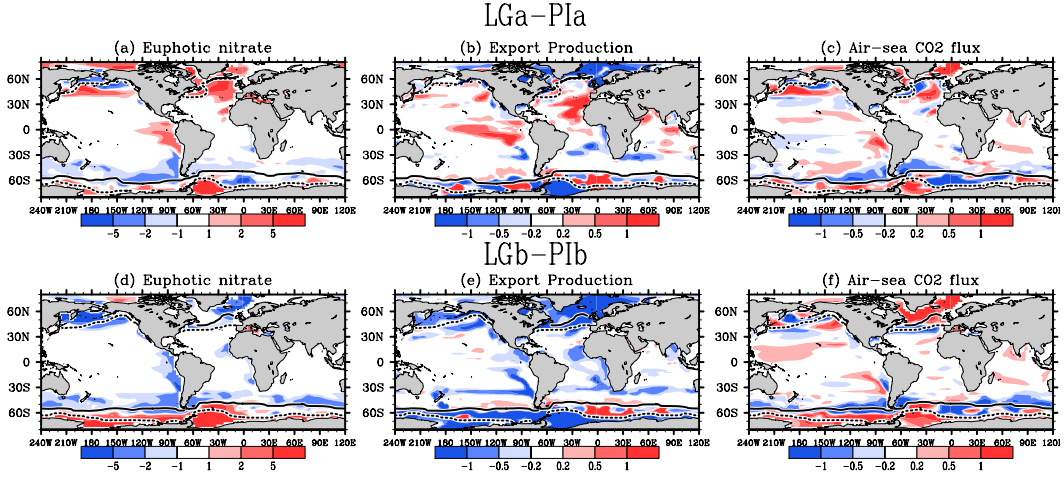

Fig. 6. Euphotic averaged nitrate anomaly (mmol m^{-3}), export POC anomaly (molC m^{-2} yr^{-2}), and air-sea CO_2 flux anomaly (mol m^{-2} yr^{-1}) **(a–c)** between LGa and PIa and **(d–f)** between LGb and PIb. Solid (dotted) lines refer to glacial sea ice fraction of 0.1 in August (February).

CPD
7, 1261–1299, 2011

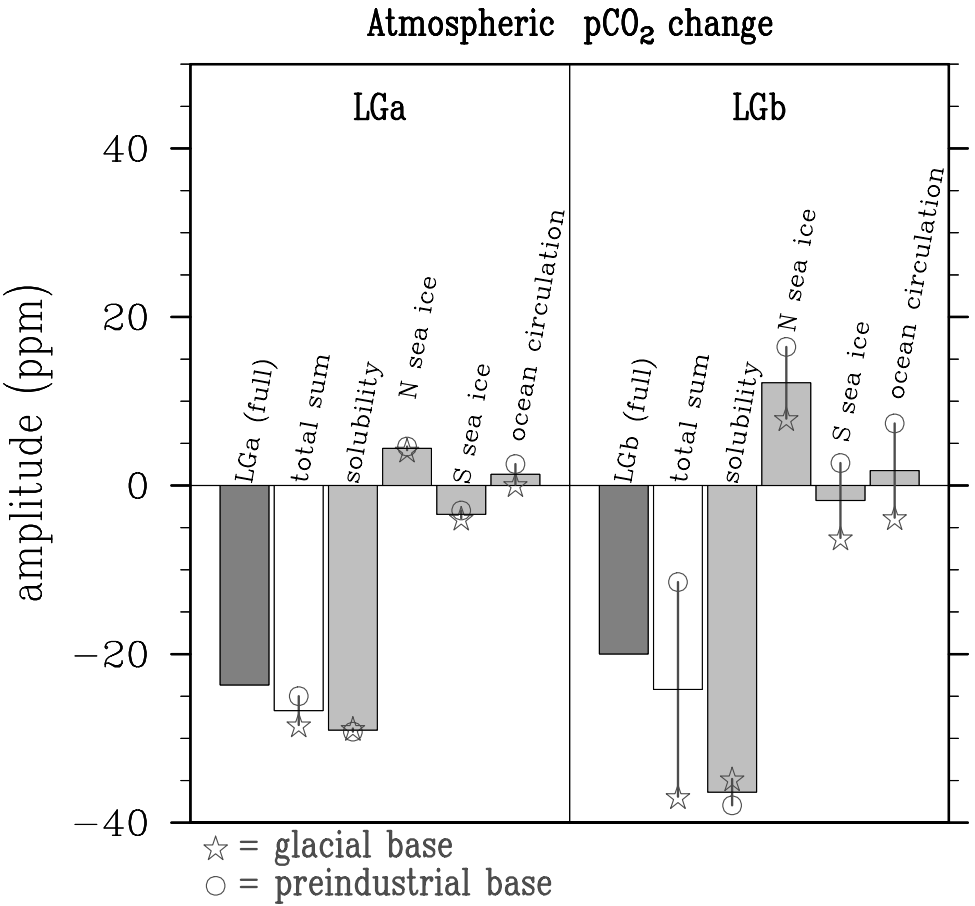

Fig. 7. Atmospheric pCO_2 responses to the climate dynamic changes of LGa and LGb. Thick bars refer to the average of two factorial estimates in the glacial and preindustrial based climates.

CPD
7, 1261–1299, 2011

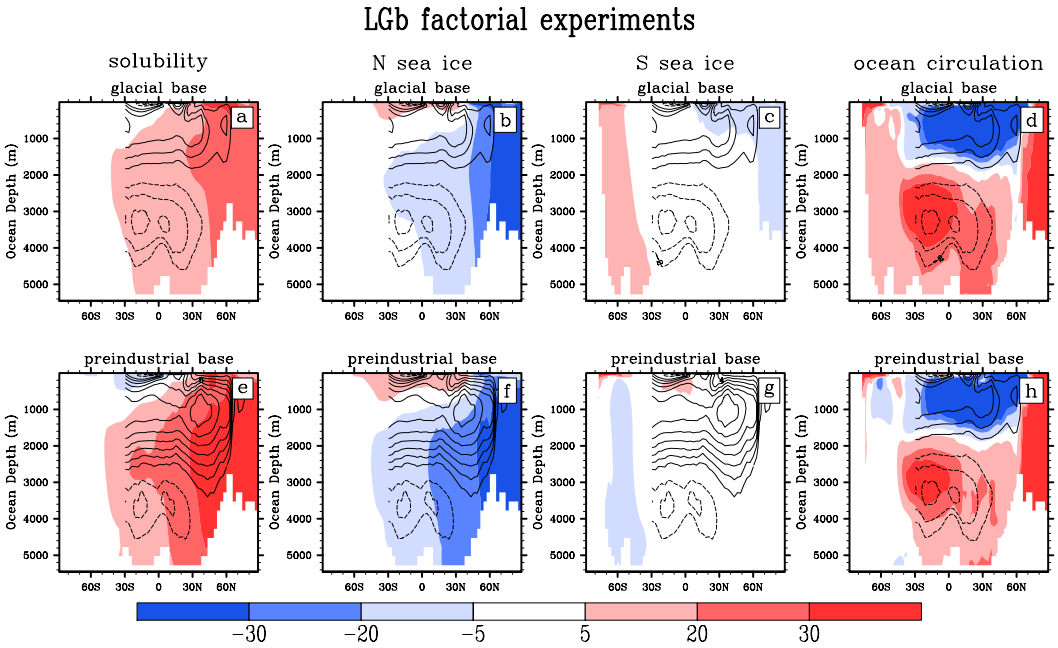

Fig. 8. Zonal-mean DIC anomalies (mmol m^{-3}) due to changes in the solubility, sea ice in the Northern and Southern Hemispheres, and ocean circulation of LGb. Upper (lower) panels correspond to results from the glacial (preindustrial) based climate. Contour lines indicate the overturning stream function of each factorial experiment. Contour intervals are 2 Sv.

CPD
7, 1261–1299, 2011

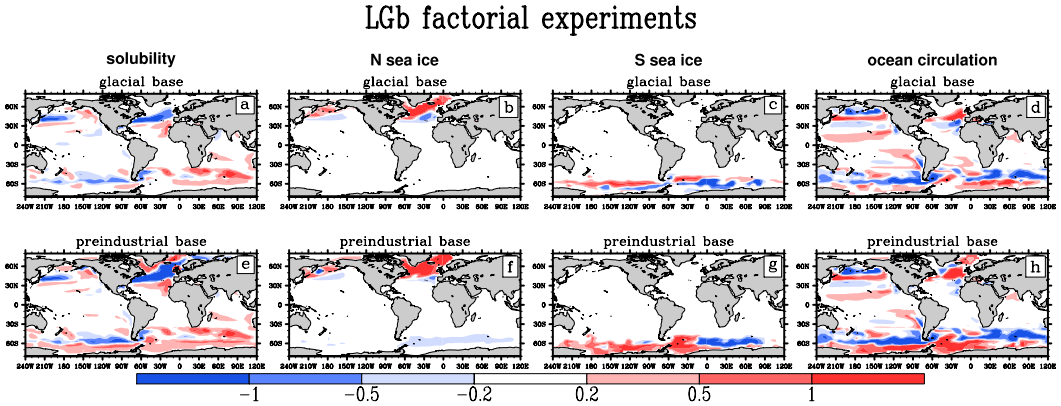

Fig. 9. Anomalous air-sea CO_2 flux (mol m^{-2} yr^{-1}) due to changes in the solubility, sea ice in the Northern and Southern Hemispheres, and ocean circulation of LGb. Upper and lower panels are as in Fig. 8.

CPD
7, 1261–1299, 2011

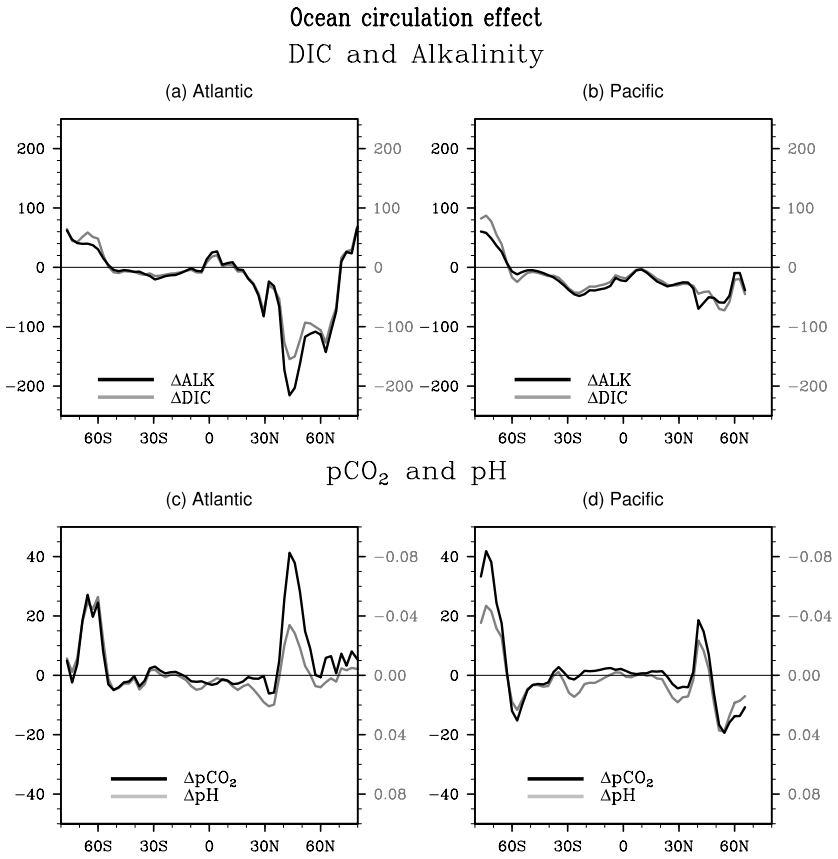

Fig. 10. (**a** and **b**) Zonal-mean ocean surface alkalinity (black) and DIC (gray) difference between LGb and LGb-oc in the Atlantic and Pacific Ocean. Panels (**c** and **d**) are the same as (**a** and **b**) except ocean surface CO_2 concentration (black) and pH (gray) anomalies are weighted by the cosine of the latitude. Units are mmol m^{-3} for ΔDIC and ΔALK, and ppm for ΔpCO_2.

CPD
7, 1261–1299, 2011